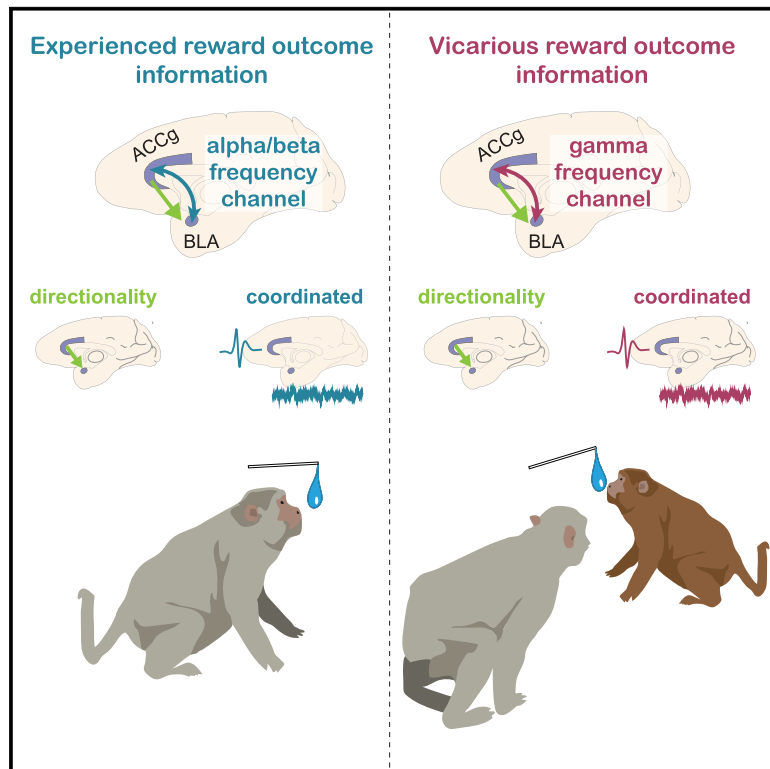


Neuron

Dissociation of vicarious and experienced rewards by coupling frequency within the same neural pathway

Graphical abstract



Authors

Philip T. Putnam, Cheng-Chi J. Chu, Nicholas A. Fagan, Olga Dal Monte, Steve W.C. Chang

Correspondence

steve.chang@yale.edu

In brief

Putnam et al. investigated specific interareal coordination between the anterior cingulate cortex and the amygdala underlying vicarious and experienced rewards arising from making social decisions. Vicarious and experienced reward outcomes were communicated using distinct frequency channels within the same shared pathway in the primate brain.

Highlights

- Vicarious and experienced reward outcomes critically shape social decisions
- Vicarious and experienced rewards distinctively engage ACC-amygdala coordination
- Different frequency channels synchronize ACC and amygdala for the two reward outcomes
- Reward outcomes prioritize information transfer from the ACC to the amygdala



Report

Dissociation of vicarious and experienced rewards by coupling frequency within the same neural pathway

Philip T. Putnam,¹ Cheng-Chi J. Chu,¹ Nicholas A. Fagan,¹ Olga Dal Monte,^{1,2} and Steve W.C. Chang^{1,3,4,5,6,*}¹Department of Psychology, Yale University, New Haven, CT 06511, USA²Department of Psychology, University of Turin, Torino, Italy³Department of Neuroscience, Yale University School of Medicine, New Haven, CT 06510, USA⁴Kavli Institute for Neuroscience, Yale University School of Medicine, New Haven, CT 06510, USA⁵Wu Tsai Institute, Yale University, New Haven, CT 06510, USA⁶Lead contact*Correspondence: steve.chang@yale.edu<https://doi.org/10.1016/j.neuron.2023.05.020>

SUMMARY

Vicarious reward, essential to social learning and decision making, is theorized to engage select brain regions similarly to experienced reward to generate a shared experience. However, it is just as important for neural systems to also differentiate vicarious from experienced rewards for social interaction. Here, we investigated the neuronal interaction between the primate anterior cingulate cortex gyrus (ACCg) and the basolateral amygdala (BLA) when social choices made by monkeys led to either vicarious or experienced reward. Coherence between ACCg spikes and BLA local field potential (LFP) selectively increased in gamma frequencies for vicarious reward, whereas it selectively increased in alpha/beta frequencies for experienced reward. These respectively enhanced couplings for vicarious and experienced rewards were uniquely observed following voluntary choices. Moreover, reward outcomes had consistently strong directional influences from ACCg to BLA. Our findings support a mechanism of vicarious reward where social agency is tagged by interareal coordination frequency within the same shared pathway.

INTRODUCTION

Altruism and prosociality are powerfully shaped by the knowledge of what other individuals experience.^{1,2} Vicarious reward, an indirectly experienced reinforcement derived from an outcome of another individual,³ contributes essentially to social learning and decision-making across many social species.⁴ Vicarious reinforcement is thought to mediate multitudes of social functions, ranging from shaping early social development³ to enabling empathy^{5,6} and to ultimately facilitating altruistic and mutually beneficial social exchanges.⁷

Vicarious processing and its behavioral effects can be explained by similar computational algorithms to those used for experienced reward.^{8–12} Evidence also supports that observing a rewarding event for a social partner elicits similar neural responses to those evoked by one's own experienced reward in overlapping cortical and subcortical areas in humans,^{13–19} non-human primates,^{20–22} and rodents.^{22–24} Of particular relevance, the anterior cingulate cortex (ACC) has emerged as a key node in processing vicarious outcomes across species.^{25,26} Single-unit recordings from ACC gyrus (ACCg) in macaques revealed a specialized function of ACCg in vicarious reward, compared with the sulcus of ACC and the orbitofrontal cortex.²⁷ Similarly,

neuroimaging in humans revealed that ACC, especially the gyrus subregion (ACCg), represents another individual's rewarding events,²⁵ and its activation level changes as a function of trait-level empathy.²⁸ Notably, bilateral excitotoxic lesions to the ventral aspects of ACC, predominantly encompassing ACCg, were shown to selectively abolish learning from vicariously rewarding events in macaques.²⁹ Relatedly, in rodents, ACC has repeatedly been found to mediate vicarious experience.^{26,30–33}

Shared neural representations between vicarious and experienced rewards may facilitate sharing other's positive or negative outcomes. At the same time, however, it is just as crucial for the neural systems involved in vicarious processing to accurately tag the social agent being directly rewarded to differentiate vicarious reward from experienced reward and guide social interaction.³⁴ How might neural systems transmit such shared yet dissociated experience? One possibility is that certain brain regions may interact in distinct manners to transmit dissociable streams of information within the core circuit implicated in vicarious computations.^{13–15,17–19}

The basolateral amygdala (BLA), a subcortical region with known functions in signaling valuation and saliency in various social contexts,^{35–40} is a good candidate that might interact with ACCg during vicarious reward.²² BLA and ACC are reciprocally



and densely interconnected, permitting efficient communications along the cortical and subcortical limbic network.⁴¹ Previous work found that decision values for vicarious and experienced rewards evoke correlated spiking activity in BLA when monkeys make prosocial choices.³⁵ These two regions were also found to coordinate neuronal activity for associative learning^{42,43} and for expressing a prosocial preference toward a social partner.³⁸ In observational fear conditioning in mice, interactions between ACC and BLA,³⁰ especially by BLA-projecting ACC neurons,³¹ were shown to be necessary for observational fear learning. However, it remains unclear how a vicariously rewarding experience engages this circuit.

Here, we examined whether and how ACCg interacts with BLA for representing vicarious and experienced rewards as macaques continuously chose to reward either themselves or their partner in a social reward allocation task, which was thought to elicit vicarious reinforcement in multiple studies.^{27,29,35,38,44,45} Our findings show that both vicarious and experienced rewards engage the same ACCg-BLA pathway, but the frequency involved in the coordination dissociates vicarious reward from experienced reward with a predominant directionality from ACCg to BLA for evaluating reward outcomes.

RESULTS

Monkeys exhibit behavioral correlates of vicarious reward

To establish behavioral correlates of vicarious reward in monkeys, we used the social reward allocation task involving pairs of rhesus macaques (*Macaca mulatta*) (an actor and a partner) (Figures 1A and 1B). This task has been applied to study the behavioral, pharmacological, single-unit, and brain lesion bases of vicarious reward in monkeys.^{27,29,35,38,44,45} On free-choice trials (Figure 1C), actors made eye movements to select one of the two targets, each mapped onto a unique reward outcome. In one context, they chose between donating a juice reward to a partner (*other*) and wasting the reward by disposing it into an empty bottle (*bottle*). In the other context, they chose between delivering themselves the reward (*self*) and delivering both themselves and the partner the same amount simultaneously (*both*). By contrast, on forced-choice trials (Figure 1C), the same reward outcomes occurred without the monkeys' choices. In this task, repeatedly showing a preference for choosing *other* over *bottle* supports vicarious reinforcement, as an actor monkey exclusively delivers a juice reward to the partner without any concurrent reward experience of the actor (i.e., the actor never directly experiences this reward).

Actors preferred *other* over *bottle* ($p < 0.0001$, Wilcoxon sign rank) and *self* over *both* ($p < 0.001$) (Figure 1D). These preferences were stable over time in each session (both $p > 0.52$, linear regression). The actors on average completed more *self/both* trials (99%) than *other/bottle* trials (87%) (Figure S1A). Notably, actors completed *other/bottle* trials when the reward size at stake was larger (small: $83\% \pm 2\%$, medium: $87\% \pm 2\%$, and large: $90\% \pm 2\%$; $F(2, 168) = 4.3$, $p = 0.02$, one-way ANOVA). Although choice reaction times were faster when actors were to be rewarded than not (Figure S1B), importantly, the high completion rate in *other/bottle* trials suggests that the actors were motivated to perform these trials even though these trials did not result in

any juice rewards to them. This choice behavior is consistent with previous studies of vicarious reward in rhesus macaques using this paradigm in different laboratories.^{27,29,35,38,44,45} Moreover, previous behavioral characterizations showed that these choices are sensitive to dominance and familiarity between pairs⁴⁴ and require the presence of a partner monkey.^{29,44} Importantly, these previous studies have found that social relationship factors modulate social preferences, rather than alter the signs of these preferences.

Gaze patterns during the free-viewing period also differed as a function of choice and gaze target (Figure S1C), and social gaze probabilities over time indicated that the actors looked at the partner more after choosing *other* than after choosing *bottle* beginning at 470 ms (mean) following reward onset (Figure 1E). By contrast, the divergence in looking at the partner for *self* and *both* appeared later at 770 ms following reward onset (Figure 1E) (difference in divergence timing: $p < 0.005$, Wilcoxon rank sum). Together, the gaze behaviors (Figures 1E and S1C) support that actors were aware of distinct reward outcomes relative to themselves or the partner.

Using this task, we previously reported that single cells in ACCg and BLA encode vicarious reward outcomes, experienced reward outcomes, or both.^{27,35,38} However, the coordination between ACCg and BLA for vicarious and experienced rewards remains unknown. Here, we recorded neural activity from 438 sites in ACCg (235 sites for monkey H and 203 sites for monkey K) and 303 sites in BLA (115 and 188 sites for monkeys H and K)⁴⁶ (Figure S1D). These data contained 253 ACCg cells (110 cells and 143 cells for monkeys H and K, respectively) and 90 BLA cells (21 cells and 69 cells for monkeys H and K, respectively) (Figure S1D). We then computed spike-field coherence between spikes in ACCg and local field potential (LFP) in BLA ($\text{ACCg}_{\text{spike}}\text{-BLA}_{\text{field}}$) and also between spikes in BLA and LFP in ACCg ($\text{BLA}_{\text{spike}}\text{-ACCg}_{\text{field}}$),^{38,47,48} resulting in 1,768 $\text{ACCg}_{\text{spike}}\text{-BLA}_{\text{field}}$ and 842 $\text{BLA}_{\text{spike}}\text{-ACCg}_{\text{field}}$ pairs. To determine specific coherence associated with vicarious reward versus experienced reward, we contrasted the coherence between *other* and *bottle* (*other-bottle*) for vicarious reward (hereafter, “partner_{norm} reward”) and between *self* and *bottle* (*self-bottle*) for reward experienced by the actors (hereafter, “actor_{norm} reward”). Given that our hypothesis-driven goal was to investigate separable neural representations of vicarious and experienced rewards, we excluded *both* condition from our analysis. To test whether coherence was selective to rewards arising from choices or whether it depended only on the outcomes themselves, we compared the coherence between free-choice and forced-choice trials. Critically, it is important to ensure that reward-related coherence results are not confounded by mouth movement artifacts of the actors. We conservatively addressed this issue by focusing on the frequency range above 10 Hz after detecting and verifying mouth movement artifacts at the lower frequency range (Figure S1E).

Vicarious, but not experienced, reward enhances gamma band coherence between ACCg spikes and BLA field

Soon after the onset of reward in free-choice trials, $\text{ACCg}_{\text{spike}}\text{-BLA}_{\text{field}}$ coherence in a low gamma frequency range (35–51 Hz) increased for partner_{norm} reward (*other-bottle*) but, intriguingly,

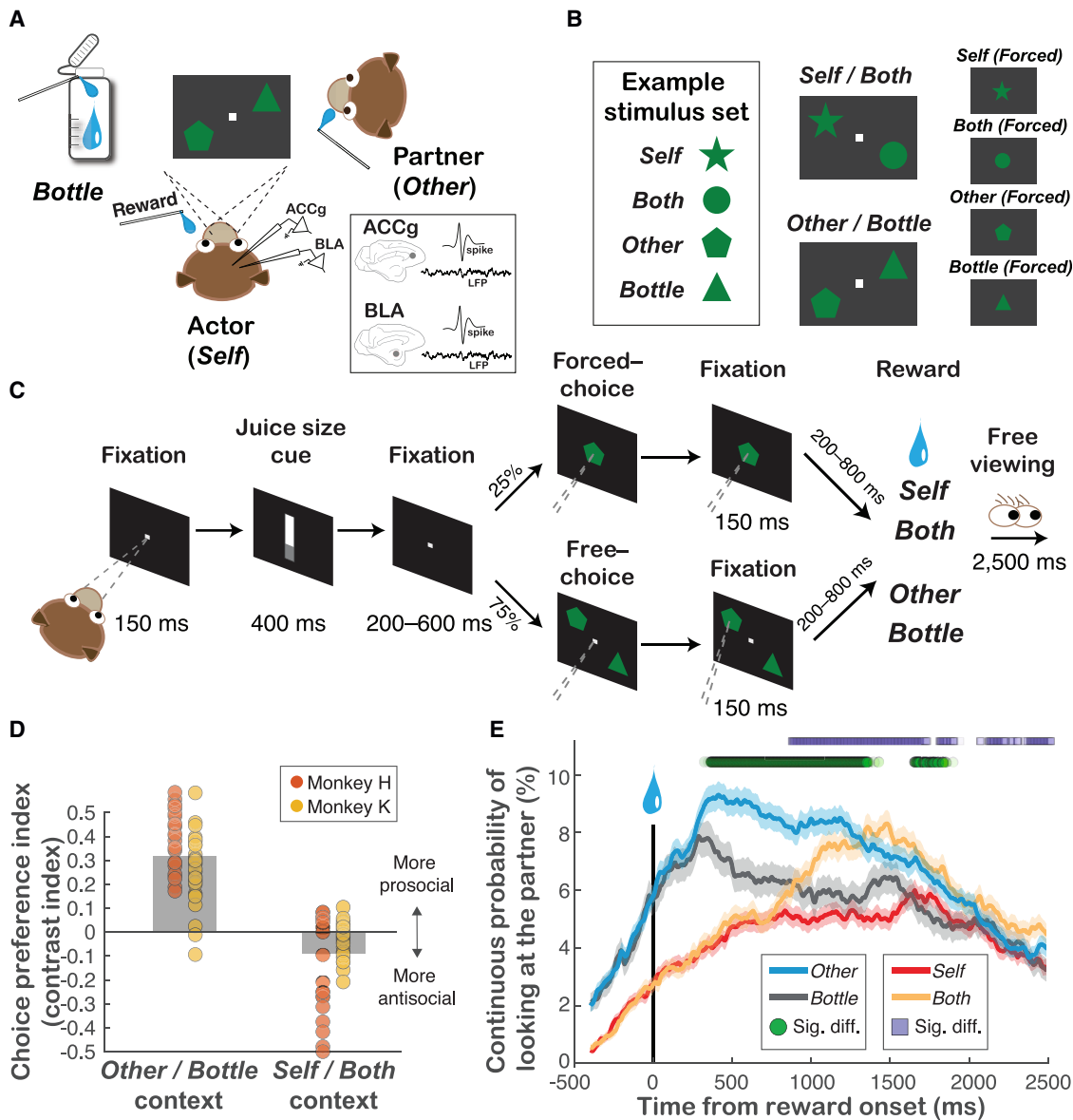


Figure 1. Monkeys show context-dependent social preferences

(A) Experimental setup involving an actor monkey (*self*), a partner monkey (*other*), and an operating juice collection bottle (*bottle*). Across 57 sessions, actors performed 298 ± 110 (mean \pm SD) trials per session (monkey H: 357 ± 121 trials per session, 31 sessions; monkey K: 227 ± 16 trials per session, 26 sessions). Spiking and local field potential (LFP) activity were collected from ACCg and BLA simultaneously (inset).

(B) Illustrations of example stimulus-reward outcome mappings for the two contexts, that is, for rewarding the actor (*self*) or both the actor and partner (*both*) (*self/both* context) and for rewarding the partner (*other*) or the bottle (*bottle*) (*other/bottle* context), and the forced-choice trial counterparts.

(C) Trial sequence for free- and forced-choice trials of the social reward allocation task.

(D) Monkeys preferred choosing *other* over *bottle* (prosocial preference) and *self* over *both* (antisocial preference). Choice preferences are expressed as averaged contrast ratios for the two contexts (*self/both* context and *other/bottle* context). Data points overlaid on top show the biases for all individual sessions for each actor.

(E) Social gaze behaviors differentiated vicarious reward from experienced reward. Continuous probability of social gaze to the partner over time (mean \pm SEM) for different types of choices aligned to reward onset. Circles and squares on top indicate bin-by-bin significant looking differences between *other* and *bottle* and between *self* and *both*, respectively ($p < 0.05$, Wilcoxon rank sum).

decreased for actor_{norm} reward (*self-bottle*) (Figures 2A and 2B). This resulted in significant coherence differences between partner_{norm} and actor_{norm} rewards in several time bins (Figure 2B). By contrast, in forced-choice trials, the gamma ACCg_{spike}-BLA_{field}

coherence showed a pronounced suppression immediately after reward onset for both reward types (Figures 2C and 2D). Moreover, the coherence values could be directly used to linearly decode actor_{norm} and partner_{norm} rewards in free-choice trials

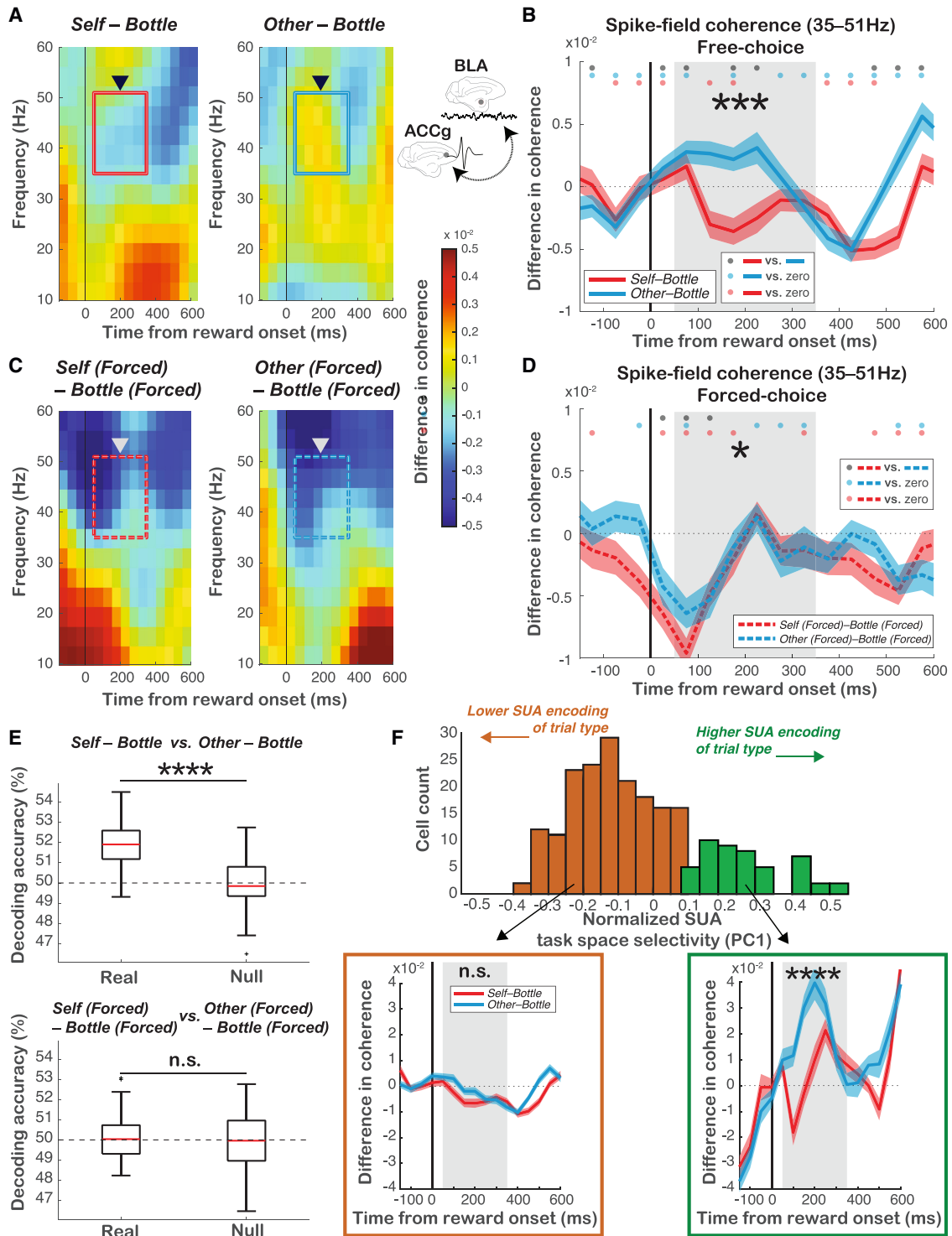


Figure 2. A selective increase of ACC_g_{spike}-BLA_{field} coherence in gamma frequency for vicarious reward but not experienced reward
 (A) Differences in ACC_g_{spike}-BLA_{field} coherence between *self* and *bottle* (left) and between *other* and *bottle* (right) across time and frequency aligned to the time of reward delivery in free-choice trials. Boxes in the spectrograms indicate the gamma frequency-time windows for analyzing actor_{norm} and partner_{norm} rewards (reward epoch, 50–350 ms from reward onset, gray shading) ($n = 1,768$ pairs).
 (B) Time courses of the gamma band (35–51 Hz) ACC_g_{spike}-BLA_{field} coherence (mean \pm SEM) for *self-bottle* (red) and *other-bottle* (blue) rewards in free-choice trials.

(legend continued on next page)

(significantly above null, $p < 0.0001$, Wilcoxon rank sum), but not in forced-choice trials ($p = 0.56$) (Figure 2E), perhaps reflecting the importance of processing partner_{norm} reward arising from social decisions. Moreover, the gamma ACCg_{spike}-BLA_{field} coherence for partner_{norm} and actor_{norm} rewards was modulated by the juice size at stake on each trial (Figure S2A). This specificity of enhanced coherence for vicarious reward in free-choice trials supports the notion that the observed coherence differences between the two reward types were not merely driven by differences in reward outcomes themselves.

We next examined whether cells with higher “task space” selectivity, based on the principal component analysis (PCA) of task variables during the reward epoch (STAR Methods), would exhibit stronger differences in the gamma ACCg_{spike}-BLA_{field} coherence between partner_{norm} and actor_{norm} rewards. We classified single cells into two categories (higher versus lower task space selectivity; k-means using PC1) and found that the selective gamma ACCg_{spike}-BLA_{field} coherence for partner_{norm} reward was predominantly found in ACCg cells with higher task space selectivity (Figure 2F). This finding was not simply due to differences in the number of cells belonging to the higher (smaller n) versus lower (larger n) task space selectivity classes, as we still observed no coherence differences between the two reward conditions when we resampled (100 times) the lower task space selective class to match the number ($p = 0.20$, two-tailed t test). Finally, this specificity for partner_{norm} reward was largely restricted to the gamma frequency range over other frequencies (Figure S2C).

Finally, we examined a relationship between spikes in BLA and LFP in ACCg (BLA_{spike}-ACC_{field}) for identical reward outcomes in the same frequencies (Figure S3). Unlike the gamma ACCg_{spike}-BLA_{field} coherence, the gamma BLA_{spike}-ACC_{field} coherence in free-choice trials showed a suppression for both partner_{norm} and actor_{norm} rewards with a greater suppression for partner_{norm} reward, thereby showing an inversed pattern from ACCg_{spike}-BLA_{field} coherence (Figure S3A). In forced-choice trials, BLA_{spike}-ACC_{field} coherence for partner_{norm} and actor_{norm} rewards did not largely differ (Figure S3B). Therefore, the gamma ACCg_{spike}-BLA_{field} coherence, but not the gamma BLA_{spike}-ACC_{field} coherence, exhibited enhanced coherence for vicarious reward.

Experienced, but not vicarious, reward enhances alpha/beta band coherence between ACCg spikes and BLA field

In contrast to the gamma coherence, ACCg_{spike}-BLA_{field} coherence in an alpha/beta frequency range (10–20 Hz) in free-choice trials increased for actor_{norm} reward (*self-bottle*), without clear

modulation for partner_{norm} reward (*other-bottle*), resulting in significant coherence differences between the two reward types in several time bins (Figure 3A). By contrast, in forced-choice trials, we again observed less clear separation between actor_{norm} and partner_{norm} rewards during the reward epoch, with no time-locked responses to reward onset (Figure 3B). Unlike the gamma band coherence, the alpha/beta ACCg_{spike}-BLA_{field} coherence exhibiting the actor_{norm} reward bias could be used to decode both free-choice and forced-choice trials (significantly above null, both $p < 0.0001$, Wilcoxon rank sum) (Figure 3C). The alpha/beta ACCg_{spike}-BLA_{field} coherence was also modulated by juice size (Figure S2B). This specificity of increased coherence for experienced reward in free-choice trials again supports the notion that the observed coherence differences between the two reward types were not merely driven by differences in reward outcomes themselves.

Intriguingly, in contrast to the gamma ACCg_{spike}-BLA_{field} coherence, ACCg cells with lower (as opposed to higher) task space selectivity during the reward epoch were associated with coherence differences in the alpha/beta band between the two rewards (Figure 3D). This finding was not simply due to differences in the number of cells belonging to the higher (smaller n) versus lower (larger n) task space selectivity classes, as we still observed no coherence differences between the two reward conditions when we resampled (100 times) the higher task space selective class to match the number ($p = 0.96$, two-tailed t test). Finally, we also examined BLA_{spike}-ACC_{field} coherence in the alpha/beta band (Figure S3). The alpha/beta BLA_{spike}-ACC_{field} coherence was overall suppressed with significantly more suppression for partner_{norm} reward than for actor_{norm} reward in free-choice trials, but this difference was not observed in forced-choice trials (Figures S3C and S3D). Therefore, the alpha/beta ACCg_{spike}-BLA_{field} coherence, but not the alpha/beta BLA_{spike}-ACC_{field} coherence, exhibited enhanced coherence for experienced reward.

Social gaze does not drive coherence differences between vicarious and experienced rewards

The actors had an opportunity to shift their gaze to look at the partner monkey after making social decisions during the free-viewing period (Figures 1E and S1C). We thus asked whether the increase in the gamma ACCg_{spike}-BLA_{field} coherence for vicarious reward was simply explained by occasional events of looking at the partner. However, aligning the same coherence to the time of looking events did not result in any difference among *self*, *other*, and *bottle* ($F(2, 1,971) = 0.93$, $p = 0.44$,

(C) Differences in ACCg_{spike}-BLA_{field} coherence between *self (forced)* and *bottle (forced)* (left) and between *other (forced)* and *bottle (forced)* (right) in forced-choice trials ($n = 1,768$ pairs). Same format as (A).

(D) Time courses of the gamma ACCg_{spike}-BLA_{field} coherence (mean \pm SEM) for *self (forced)*-*bottle (forced)* (red) and *other (forced)*-*bottle (forced)* (blue) in forced-choice trials. In (B) and (D), circles at the top indicate unsmoothed raw time bins for significant differences between the two traces (dark gray, $p < 0.05$, two-tailed t test) and of each trace against zero (matching colors, $p < 0.05$, two-tailed t test).

(E) Decoding of partner_{norm} and actor_{norm} rewards (linear discriminant analysis [LDA]) using the coherence values from the reward epoch for the gamma coherence for free-choice (top) and forced-choice (bottom) trials. Asterisks indicate a significant difference between the real and null data (**** $p < 0.0001$, n.s., not significant; Wilcoxon rank sum).

(F) (Top) Normalized distribution single-unit activity (SUA) task space selectivity of ACCg cells from PCA (PC1) (STAR Methods). Two colors represent classification results for those with higher (green) or lower (orange) task space selectivity (k-means). (Bottom) Differences in the gamma ACCg_{spike}-BLA_{field} coherence (mean \pm SEM) for *self-bottle* and *other-bottle* by ACCg cells with higher or lower SUA task space selectivity. In (B), (D), and (F), asterisks indicate a significant difference between the two traces for the reward epoch (gray shading, 50–350 ms; **** $p < 0.0001$, *** $p < 0.0005$; * $p = 0.02$, n.s., not significant; two-tailed t test).

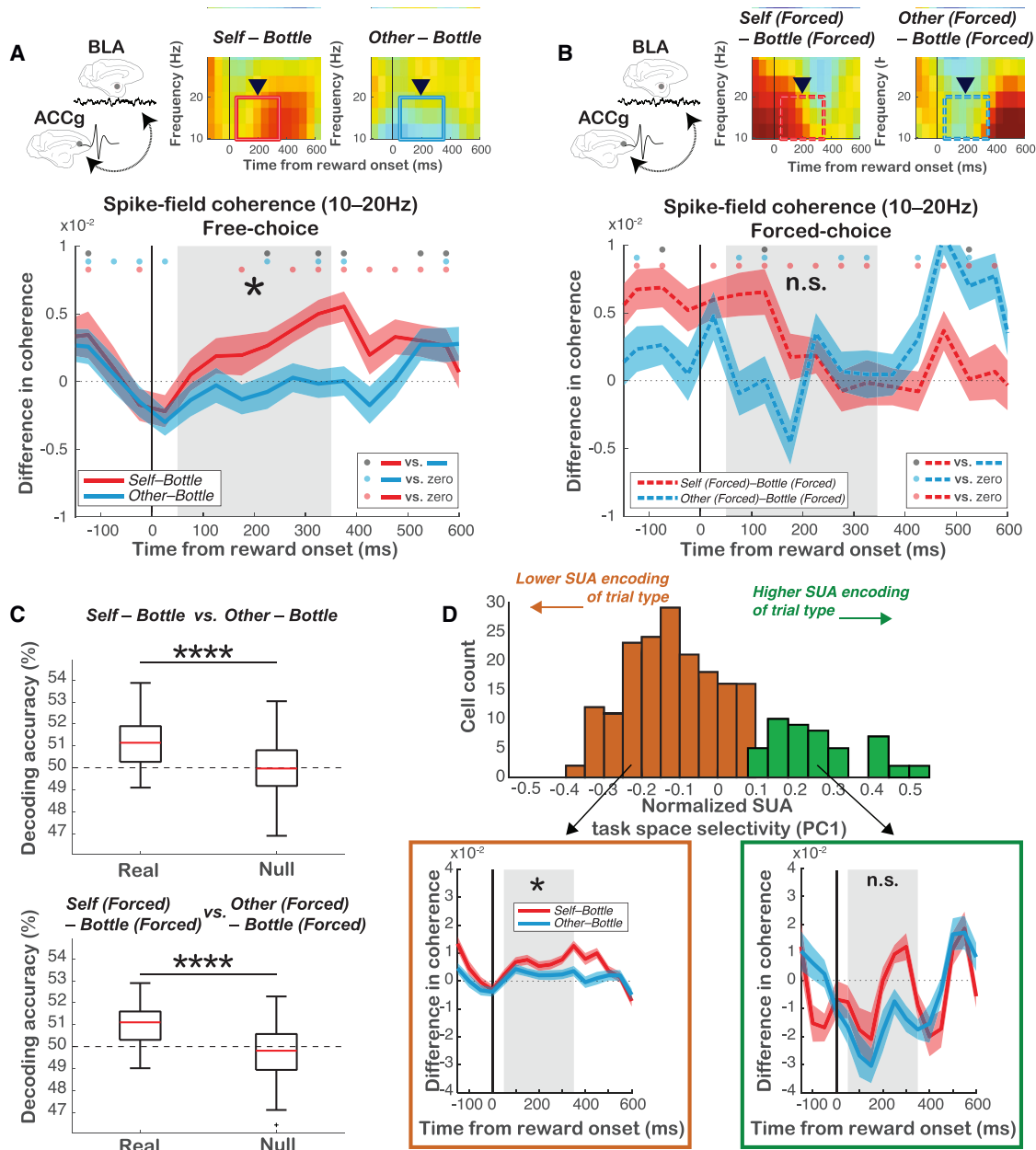


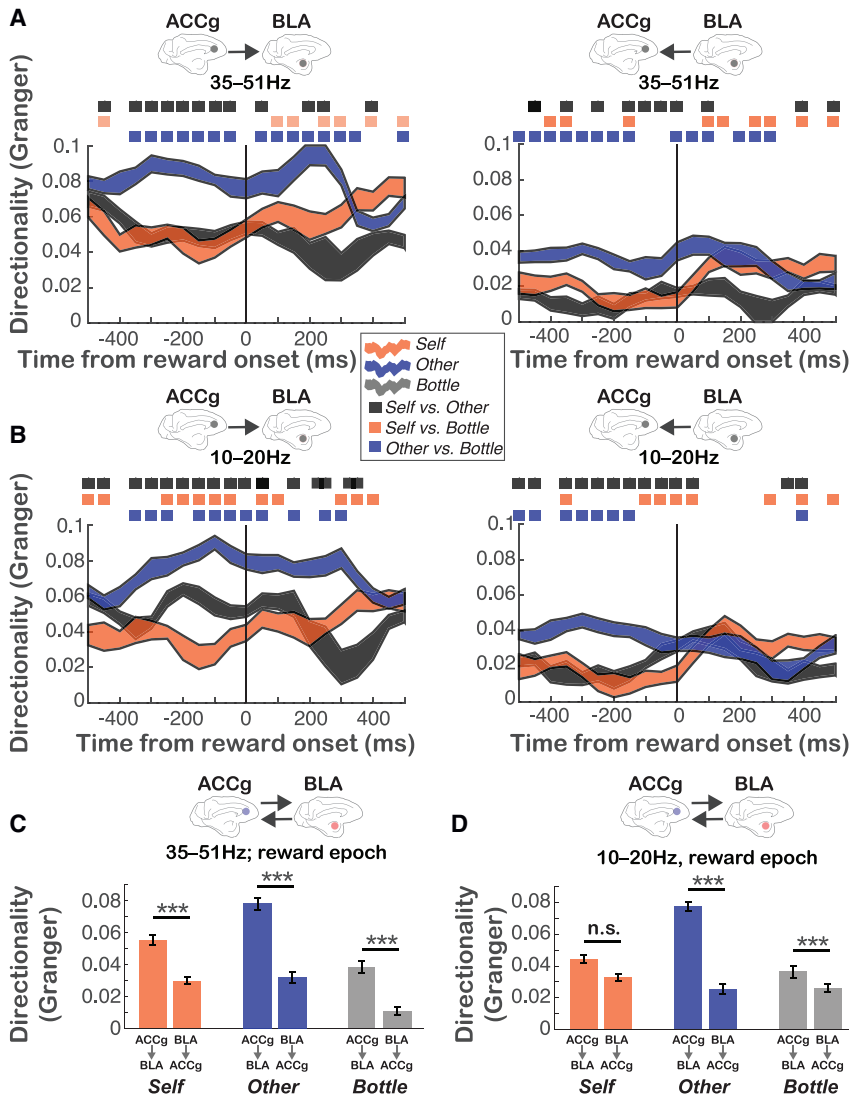
Figure 3. A selective increase of ACCg_{spike}-BLA_{field} coherence in alpha/beta frequency for actor's experienced reward but not vicarious reward

(A) Time courses of the alpha/beta band (10–20 Hz) ACCg_{spike}-BLA_{field} coherence (mean ± SEM) for *self-bottle* (red) and *other-bottle* (blue) rewards in free-choice trials (n = 1,768 pairs). Insets on top show the alpha/beta frequency-time windows from the same spectrograms in Figure 2A.

(B) Time courses of the alpha/beta ACCg_{spike}-BLA_{field} coherence (mean ± SEM) for *self (forced)-bottle (forced)* (red) and *other (forced)-bottle (forced)* (blue) in forced-choice trials (n = 1,768 pairs). Insets on top show the relevant frequency-time windows (from Figure 2C). In (A) and (B), circles at the top indicate unsmoothed raw time bins for significant differences between the two traces (dark gray, p < 0.05, two-tailed t test) and of each trace against zero (matching colors, p < 0.05, two-tailed t test).

(C) Decoding of actor_{norm} and partner_{norm} rewards (LDA) using the coherence values from the reward epoch for the alpha/beta coherence for free-choice (top) and forced-choice (bottom) trials. Asterisks indicate a significant difference between the real and null data (****p < 0.0001, Wilcoxon rank sum).

(D) (Top) Normalized distribution SUA task space selectivity of ACCg cells from PCA (PC1). Two colors represent classification results for those with higher (green) or lower (orange) task space selectivity (k-means). (Bottom) Differences in the alpha/beta ACCg_{spike}-BLA_{field} coherence (mean ± SEM) for *self-bottle* and *other-bottle* by ACCg cells with higher or lower SUA task space selectivity. In (A), (B), and (D), asterisks indicate a significant difference between the two traces for the reward epoch (gray shading, 50–350 ms; *p < 0.05; n.s., not significant; two-tailed t test).



one-way ANOVA; Figures S4A and S4C) or between *self-bottle* and *other-bottle* contrasts ($p = 0.89$, two-tailed t test), for a comparable 50–350 ms epoch, supporting the notion that social gaze behaviors were not underlying the coherence differences between vicarious and experienced rewards. Similarly, we asked the same question for the alpha/beta ACCg_{spike}-BLA_{field} coherence. Again, aligning the same coherence to the time of looking events did not result in any difference among *self*, *other*, and *bottle* ($F(2, 1,971) = 1.69$, $p = 0.18$, one-way ANOVA; Figures S4B and S4C). Although the contrast between *self-bottle* (-0.005 ± 0.002 [mean \pm SEM]) and *other-bottle* (0.001 ± 0.002) in this frequency range reached significance ($p = 0.05$, two-tailed t test), these values (i.e., the negative value for *self-bottle* and the smaller value for *self-bottle* compared with *other-bottle*) cannot explain the reward epoch findings for the alpha/beta ACCg_{spike}-BLA_{field} coherence, which showed larger and above-zero coherence for *self-bottle* than for *other-bottle*. These results support that social gaze behaviors did not drive the observed coherence differences.

Figure 4. Directionality biases for vicarious and experienced rewards in the ACCg-BLA pathway

(A and B) Granger directionality value for the gamma (A) and alpha/beta frequency ranges (B) over time aligned to the time of reward delivery for *self* (orange), *other* (dark blue), and *bottle* (dark gray) outcomes separately (line width: mean \pm SEM). In (A) and (B), the left and right panels show directionality values for ACCg \rightarrow BLA and BLA \rightarrow ACCg, respectively. Rectangles on top indicate unsmoothed raw time bins with significant differences in the contrasted Granger directionality values between *self* and *other* (dark gray), *self* and *bottle* (orange), and *other* and *bottle* (dark blue) ($p < 0.05$, two-tailed t test).

(C and D) Average Granger values (mean \pm SEM) of the ACCg \rightarrow BLA and BLA \rightarrow ACCg directions from the reward epoch for the gamma (C) and alpha/beta bands (D). Asterisks indicate a significant difference between the two directions (** $p < 0.001$, n.s., not significant, two-tailed t test).

Reward outcome is associated with strong directionality from ACCg to BLA

ACCg and BLA are densely connected bidirectionally.⁴¹ Accumulating evidence suggests that social interactions are associated with a bias in directional influence among interconnected regions.^{38,49–51} To examine potential bias in the directional influence of either ACCg or BLA for vicarious reward, we performed a Granger directionality analysis using continuous LFP signals in the gamma and alpha/beta ranges (STAR Methods). For both frequency ranges, *other*, compared with *self* or *bottle* outcome, was associated with greater directionality overall from ACCg to BLA (ACCg \rightarrow BLA) (Figures 4A and 4B). Notably, ACCg \rightarrow BLA directionality for *other* was greater than the opposite directionality (BLA \rightarrow ACCg) for *other* for both frequency ranges (reward epoch: both $p < 0.001$, two-tailed t test) (Figures 4C and 4D). However, it is important to note that such directionality bias was not exclusively found for *other*—for example, in the gamma band, both *self* and *bottle* showed the ACCg \rightarrow BLA bias during the reward epoch (both $p < 0.001$), suggesting that reward-outcome-related information consistently exhibited the ACCg \rightarrow BLA bias. By applying the partial directed coherence (PDC, STAR Methods), we largely replicated the consistent ACCg \rightarrow BLA directionality bias for *self*, *other*, and *bottle* reward outcomes, albeit with some differences in tested condition magnitudes and frequency band magnitudes compared with the Granger results (Figures S4D and S4E).

DISCUSSION

A dominant theory of vicarious processing is that other's outcomes are represented in a similar manner to experienced

outcomes.^{16,17,19,27,32,35,52–54} Our results provide neuronal evidence of interareal ACCg-BLA coordination for vicarious reward. Importantly, within the very same ACCg_{spike}-BLA_{field} pairs, distinct frequency ranges were selectively engaged for vicarious reward versus experienced reward. The ACCg_{spike}-BLA_{field} coherence in the gamma band was enhanced for vicarious reward to differentiate it from experienced reward, whereas the ACCg_{spike}-BLA_{field} coherence in the alpha/beta band was increased for experienced reward to differentiate it from vicarious reward. These data, therefore, suggest that distinct frequency channels within the same ACCg-BLA pathway are used to dissociate vicarious and experienced rewards. Such dissociations within the shared pathway may be useful for “tagging” social agency during reward-guided social interactions. Overall, our finding supports the notion that there are frequency modules within the same ACCg-BLA circuit that are functionally segregated to process either vicarious reward outcome or experienced reward outcome.

Continuously completing *other/bottle* trials in the absence of any direct reinforcement is a central feature of the current task.^{44,45} Crucially, distinct coordination patterns for vicarious and experienced rewards were largely selective to trials in which monkeys made preferred choices, suggesting that vicarious reward from expressing social preferences may uniquely synchronize the two neural populations. It also supports the importance of choosing to be generous in experiencing vicarious reward.

In a previous work measuring dopamine release in the ventral striatum of rats as they observed reward delivery to a conspecific, ACC neurons signaled reward or shock delivered to the conspecific.²⁴ Moreover, the rat ACC contains neurons that similarly represent experienced and vicarious pain,³² supporting the role of ACC in affective empathy.⁵ The current findings in monkeys extend and refine this knowledge. Specifically, we report that the same ACCg-BLA pathway dissociates vicarious reward from experienced reward through distinct coupling dynamics. The ACCg-BLA pathway may thus implement shared yet also dissociable information streams underlying vicarious and experienced rewards to guide social learning and decision-making as well as empathy, which requires both shared and separate understanding between self and others.⁵⁵

We observed a clear directionality bias from ACCg to BLA during the reward outcome period. Interestingly, this bias was pronounced for all the reward outcomes examined (even for *bottle* outcome), suggesting that this information directionality mode is dominant for evaluating reward outcomes in the ACCg-BLA pathway. This is consistent with findings in mice demonstrating that BLA-projecting ACC population is necessary for observational fear learning³¹ and that synchronization between ACC and BLA is related to observational fear learning.³⁰ Our results support the notion that ACCg-BLA interaction in the primate brain is implicated in processing vicarious reward, extending studies in rodents that have examined the role of ACC-BLA interaction in processing vicariously aversive outcomes.^{30,31}

Accumulating evidence from whole-brain functional neuroimaging in humans and macaques supports that several brain regions, including ACCg and BLA, are consistently recruited for multitudes of social cognitive operations.^{16,18,22,25,56–61} In the

context of what is referred to as the “social brain,” our findings propose an intriguing possibility that shared representations of self and others in some of these social brain areas could be dissociated into two streams of information by network-level interactions. Such a shared yet dissociable mechanism may promote empathic accuracy by tagging social agency for reward (vicarious or experienced) using frequency within the same neural pathway.

STAR★METHODS

Detailed methods are provided in the online version of this paper and include the following:

- KEY RESOURCES TABLE
- RESOURCE AVAILABILITY
 - Lead contact
 - Materials availability
 - Data and code availability
- EXPERIMENTAL MODEL AND SUBJECT DETAILS
 - Animals and surgery
 - Anatomical localization
 - Social reward allocation task
 - Electrophysiological recordings
 - Method details

SUPPLEMENTAL INFORMATION

Supplemental information can be found online at <https://doi.org/10.1016/j.neuron.2023.05.020>.

ACKNOWLEDGMENTS

We are extremely grateful to Bijan Pesaran for his guidance in examining oscillatory neural processes throughout the duration of this research. We also thank Daeyeol Lee and Alex Kwan for their thoughtful discussions and suggestions on this line of work. We are also grateful to Weikang Shi and Olivia Meisner for their helpful comments on the manuscript and discussions of the results. This work was either fully or in part supported by the National Institute of Mental Health (R01MH110750, R01MH120081, R21MH107853, and R00MH099093), Alfred P. Sloan Foundation (FG-2015-66028), and Teresa Seessel Postdoctoral Fellowship.

AUTHOR CONTRIBUTIONS

S.W.C.C. and O.D.M. designed the study, and S.W.C.C. and P.T.P. wrote the paper. O.D.M. collected the data. P.T.P., N.A.F., C.-C.J.C., and S.W.C.C. analyzed the data.

DECLARATION OF INTERESTS

The authors declare no competing interests.

INCLUSION AND DIVERSITY

We support inclusive, diverse, and equitable conduct of research.

Received: January 5, 2023

Revised: April 5, 2023

Accepted: May 24, 2023

Published: June 21, 2023

REFERENCES

- Preston, S.D., and de Waal, F.B.M. (2002). Empathy: Its ultimate and proximate bases. *discussion 20. Behav. Brain Sci.* *25*, 1–20.
- Tomasello, M., Carpenter, M., Call, J., Behne, T., and Moll, H. (2005). Understanding and sharing intentions: the origins of cultural cognition. *discussion 691–735. Behav. Brain Sci.* *28*, 675–691.
- Bandura, A., Ross, D., and Ross, S.A. (1963). Vicarious reinforcement and imitative learning. *J. Abnorm. Psychol.* *67*, 601–607.
- Heyes, C.M. (1994). Social Learning in Animals: Categories and Mechanisms. *Biol. Rev. Camb. Philos. Soc.* *69*, 207–231.
- Singer, T., and Lamm, C. (2009). The Social Neuroscience of Empathy. *Ann. N. Y. Acad. Sci.* *1156*, 81–96.
- Zaki, J., Wager, T.D., Singer, T., Keyesers, C., and Gazzola, V. (2016). The Anatomy of Suffering: Understanding the Relationship between Nociceptive and Empathic Pain. *Trends Cogn. Sci.* *20*, 249–259.
- Park, S.Q., Kahnt, T., Dogan, A., Strang, S., Fehr, E., and Tobler, P.N. (2017). A neural link between generosity and happiness. *Nat. Commun.* *8*, 15964.
- Apps, M.A.J., Lesage, E., and Ramnani, N. (2015). Vicarious Reinforcement Learning Signals When Instructing Others. *J. Neurosci.* *35*, 2904–2913.
- Charpentier, C.J., and O’Doherty, J.P. (2018). The Application of Computational Models to Social Neuroscience: Promises and Pitfalls. *Soc. Neurosci.* *13*, 637–647.
- Lee, D. (2008). Game theory and neural basis of social decision making. *Nat. Neurosci.* *11*, 404–409.
- Lockwood, P.L., Apps, M.A.J., Valton, V., Viding, E., and Roiser, J.P. (2016). Neurocomputational mechanisms of prosocial learning and links to empathy. *Proc. Natl. Acad. Sci. USA* *113*, 9763–9768.
- Olsson, A., Knapska, E., and Lindström, B. (2020). The neural and computational systems of social learning. *Nat. Rev. Neurosci.* *21*, 197–212.
- Harbaugh, W.T., Mayr, U., and Burghart, D.R. (2007). Neural Responses to Taxation and Voluntary Giving Reveal Motives for Charitable Donations. *Science* *316*, 1622–1625.
- Lieberman, M.D. (2007). Social cognitive neuroscience: a review of core processes. *Annu. Rev. Psychol.* *58*, 259–289.
- Behrens, T.E.J., Hunt, L.T., and Rushworth, M.F.S. (2009). The Computation of Social Behavior. *Science* *324*, 1160–1164.
- Mobbs, D., Yu, R., Meyer, M., Passamonti, L., Seymour, B., Calder, A.J., Schweizer, S., Frith, C.D., and Dalgleish, T. (2009). A Key Role for Similarity in Vicarious Reward. *Science* *324*, 900.
- Fareri, D.S., and Delgado, M.R. (2014). Social Rewards and Social Networks in the Human Brain. *Neuroscientist* *20*, 387–402.
- Ruff, C.C., and Fehr, E. (2014). The neurobiology of rewards and values in social decision making. *Nat. Rev. Neurosci.* *15*, 549–562.
- Morelli, S.A., Sacchet, M.D., and Zaki, J. (2015). Common and distinct neural correlates of personal and vicarious reward: A quantitative meta-analysis. *NeuroImage* *112*, 244–253.
- Chang, S.W.C., Brent, L.J.N., Adams, G.K., Klein, J.T., Pearson, J.M., Watson, K.K., and Platt, M.L. (2013). Neuroethology of primate social behavior. *Proc. Natl. Acad. Sci. USA* *110*, 10387–10394.
- Wittmann, M.K., Lockwood, P.L., and Rushworth, M.F.S. (2018). Neural mechanisms of social cognition in primates. *Annu. Rev. Neurosci.* *41*, 99–118.
- Gangopadhyay, P., Chawla, M., Dal Monte, O., and Chang, S.W.C. (2021). Prefrontal-amygdala circuits in social decision-making. *Nat. Neurosci.* *24*, 5–18.
- Chen, P., and Hong, W. (2018). Neural circuit mechanisms of social behavior. *Neuron* *98*, 16–30.
- Kashtelyan, V., Lichtenberg, N.T., Chen, M.L., Cheer, J.F., and Roesch, M.R. (2014). Observation of reward delivery to a conspecific modulates dopamine release in ventral striatum. *Curr. Biol.* *24*, 2564–2568.
- Apps, M.A.J., Rushworth, M.F.S., and Chang, S.W.C. (2016). The Anterior Cingulate Gyrus and Social Cognition: Tracking the Motivation of Others. *Neuron* *90*, 692–707.
- Burgos-Robles, A., Gothard, K.M., Monfils, M.H., Morozov, A., and Vicentic, A. (2019). Conserved features of anterior cingulate networks support observational learning across species. *Neurosci. Biobehav. Rev.* *107*, 215–228.
- Chang, S.W.C., Gariépy, J.F., and Platt, M.L. (2013). Neuronal reference frames for social decisions in primate frontal cortex. *Nat. Neurosci.* *16*, 243–250.
- Lockwood, P.L., Apps, M.A.J., Roiser, J.P., and Viding, E. (2015). Encoding of Vicarious Reward Prediction in Anterior Cingulate Cortex and Relationship with Trait Empathy. *J. Neurosci.* *35*, 13720–13727.
- Basile, B.M., Schafroth, J.L., Karaskiewicz, C.L., Chang, S.W.C., and Murray, E.A. (2020). The anterior cingulate cortex is necessary for forming prosocial preferences from vicarious reinforcement in monkeys. *PLoS Biol.* *18*, e3000677.
- Jeon, D., Kim, S., Chetana, M., Jo, D., Ruley, H.E., Lin, S.-Y., Rabah, D., Kinet, J.-P., and Shin, H.-S. (2010). Observational fear learning involves affective pain system and Cav1.2 Ca²⁺ channels in ACC. *Nat. Neurosci.* *13*, 482–488.
- Allsop, S.A., Wichmann, R., Mills, F., Burgos-Robles, A., Chang, C.J., Felix-Ortiz, A.C., Vienne, A., Beyeler, A., Izadmehr, E.M., Glover, G., et al. (2018). Corticoamygdala Transfer of Socially Derived Information Gates Observational Learning. *Cell* *173*, 1329–1342.e18.
- Carrillo, M., Han, Y., Migliorati, F., Liu, M., Gazzola, V., and Keyesers, C. (2019). Emotional Mirror Neurons in the Rat’s Anterior Cingulate Cortex. *Curr. Biol.* *29*, 1301–1312.e6.
- Schneider, K.N., Sciarillo, X.A., Nudelman, J.L., Cheer, J.F., and Roesch, M.R. (2020). Anterior Cingulate Cortex Signals Attention in a Social Paradigm that Manipulates Reward and Shock. *Curr. Biol.* *30*, 3724–3735.e2.
- Báez-Mendoza, R., Mastrobattista, E.P., Wang, A.J., and Williams, Z.M. (2021). Social agent identity cells in the prefrontal cortex of interacting groups of primates. *Science* *374*, eabb4149.
- Chang, S.W., Fagan, N.A., Toda, K., Utevsky, A.V., Pearson, J.M., and Platt, M.L. (2015). Neural mechanisms of social decision-making in the primate amygdala. *Proc. Natl. Acad. Sci. USA* *112*, 16012–16017.
- Munuera, J., Rigotti, M., and Salzman, C.D. (2018). Shared neural coding for social hierarchy and reward value in primate amygdala. *Nat. Neurosci.* *21*, 415–423.
- Grabenhorst, F., Báez-Mendoza, R., Genest, W., Deco, G., and Schultz, W. (2019). Primate Amygdala Neurons Simulate Decision Processes of Social Partners. *Cell* *177*, 986–998.e15.
- Dal Monte, O., Chu, C.C.J., Fagan, N.A., and Chang, S.W.C. (2020). Specialized medial prefrontal-amygdala coordination in other-regarding decision preference. *Nat. Neurosci.* *23*, 565–574.
- Gothard, K.M. (2020). Multidimensional processing in the amygdala. *Nat. Rev. Neurosci.* *21*, 565–575.
- Hernandez-Lllement, J., van Wingerden, M., Schäble, S., and Kalenscher, T. (2016). Basolateral amygdala lesions abolish mutual reward preferences in rats. *Neurobiol. Learn. Mem.* *127*, 1–9.
- Carmichael, S.T., and Price, J.L. (1995). Limbic connections of the orbital and medial prefrontal cortex in macaque monkeys. *J. Comp. Neurol.* *363*, 615–641.
- Klavir, O., Genud-Gabai, R., and Paz, R. (2013). Functional Connectivity between Amygdala and Cingulate Cortex for Adaptive Aversive Learning. *Neuron* *80*, 1290–1300.

43. Taub, A.H., Perets, R., Kahana, E., and Paz, R. (2018). Oscillations Synchronize Amygdala-to-Prefrontal Primate Circuits during Aversive Learning. *Neuron* 97, 291–298.e3.
44. Chang, S.W.C., Wincoff, A.A., and Platt, M.L. (2011). Vicarious Reinforcement in Rhesus Macaques (*Macaca mulatta*). *Front. Neurosci.* 5, 27.
45. Chang, S.W.C., Barter, J.W., Ebitz, R.B., Watson, K.K., and Platt, M.L. (2012). Inhaled oxytocin amplifies both vicarious reinforcement and self reinforcement in rhesus macaques (*Macaca mulatta*). *Proc. Natl. Acad. Sci. USA* 109, 959–964.
46. Paxinos, G., Huang, X.-F., and Toga, A.W. (1999). *The Rhesus Monkey Brain in Stereotaxic Coordinates*, First Edition (Academic Press).
47. Womelsdorf, T., Fries, P., Mitra, P.P., and Desimone, R. (2006). Gamma-band synchronization in visual cortex predicts speed of change detection. *Nature* 439, 733–736.
48. Pesaran, B., Nelson, M.J., and Andersen, R.A. (2008). Free choice activates a decision circuit between frontal and parietal cortex. *Nature* 453, 406–409.
49. Noritake, A., Ninomiya, T., and Isoda, M. (2018). Social reward monitoring and valuation in the macaque brain. *Nat. Neurosci.* 21, 1452–1462.
50. Noritake, A., Ninomiya, T., and Isoda, M. (2020). Representation of distinct reward variables for self and other in primate lateral hypothalamus. *Proc. Natl. Acad. Sci. USA* 117, 5516–5524.
51. Ninomiya, T., Noritake, A., Kobayashi, K., and Isoda, M. (2020). A causal role for frontal cortico-cortical coordination in social action monitoring. *Nat. Commun.* 11, 5233.
52. van Gorp, S., Hoog, J., Kalenscher, T., and van Wingerden, M. (2020). Vicarious reward unblocks associative learning about novel cues in male rats. *eLife* 9, e60755.
53. Hackel, L.M., Zaki, J., and Van Bavel, J.J. (2017). Social identity shapes social valuation: evidence from prosocial behavior and vicarious reward. *Soc. Cogn. Affect. Neurosci.* 12, 1219–1228.
54. Olsson, A., McMahon, K., Papenberg, G., Zaki, J., Bolger, N., and Ochsner, K.N. (2016). Vicarious Fear Learning Depends on Empathic Appraisals and Trait Empathy. *Psychol. Sci.* 27, 25–33.
55. Lamm, C., Bukowski, H., and Silani, G. (2016). From shared to distinct self–other representations in empathy: evidence from neurotypical function and socio-cognitive disorders. *Philos. Trans. R. Soc. Lond. B Biol. Sci.* 371, 20150083.
56. Hampton, A.N., Bossaerts, P., and O’Doherty, J.P. (2008). Neural correlates of mentalizing-related computations during strategic interactions in humans. *Proc. Natl. Acad. Sci. USA* 105, 6741–6746.
57. Sallet, J., Mars, R.B., Noonan, M.P., Andersson, J.L., O’Reilly, J.X., Jbabdi, S., Croxson, P.L., Jenkinson, M., Miller, K.L., and Rushworth, M.F.S. (2011). Social Network Size Affects Neural Circuits in Macaques. *Science* 334, 697–700.
58. Smith, D.V., Clithero, J.A., Boltuck, S.E., and Huettel, S.A. (2014). Functional connectivity with ventromedial prefrontal cortex reflects subjective value for social rewards. *Soc. Cogn. Affect. Neurosci.* 9, 2017–2025.
59. Shimada, S., Matsumoto, M., Takahashi, H., Yomogida, Y., and Matsumoto, K. (2016). Coordinated activation of premotor and ventromedial prefrontal cortices during vicarious reward. *Soc. Cogn. Affect. Neurosci.* 11, 508–515.
60. Sliwa, J., and Freiwald, W.A. (2017). A dedicated network for social interaction processing in the primate brain. *Science* 356, 745–749.
61. Freiwald, W.A. (2020). Social interaction networks in the primate brain. *Curr. Opin. Neurobiol.* 65, 49–58.
62. Brainard, D.H. (1997). The psychophysics Toolbox. *Spat. Vis.* 10, 433–436.
63. Cornelissen, F.W., Peters, E.M., and Palmer, J. (2002). The EyeLink Toolbox: eye tracking with MATLAB and the Psychophysics Toolbox. *Behav. Res. Methods, Instrum. Comput.* 34, 613–617.
64. Krassanakis, V., Filippakopoulou, V., and Nakos, B. (2014). EyeMMV toolbox: An eye movement post-analysis tool based on a two-step spatial dispersion threshold for fixation identification. *J. Eye Mov. Res.* 7.
65. Chung, J.E., Magland, J.F., Barnett, A.H., Tolosa, V.M., Tooker, A.C., Lee, K.Y., Shah, K.G., Felix, S.H., Frank, L.M., and Greengard, L.F. (2017). A Fully Automated Approach to Spike Sorting. *Neuron* 95, 1381–1394.e6.
66. Liu, Y., Yttri, E.A., and Snyder, L.H. (2010). Intention and attention: different functional roles for LIPd and LIPv. *Nat. Neurosci.* 13, 495–500.
67. Bokil, H., Andrews, P., Kulkarni, J.E., Mehta, S., and Mitra, P.P. (2010). Chronux: a platform for analyzing neural signals. *J. Neurosci. Methods* 192, 146–151.
68. Bastos, A.M., and Schoffelen, J.-M. (2015). A Tutorial Review of Functional Connectivity Analysis Methods and Their Interpretational Pitfalls. *Front. Syst. Neurosci.* 9, 175.
69. Jarvis, M.R., and Mitra, P.P. (2001). Sampling properties of the spectrum and coherency of sequences of action potentials. *Neural Comput.* 13, 717–749.
70. Rainer, G., Asaad, W.F., and Miller, E.K. (1998). Selective representation of relevant information by neurons in the primate prefrontal cortex. *Nature* 393, 577–579.
71. Minxha, J., Mosher, C., Morrow, J.K., Mamelak, A.N., Adolphs, R., Gothard, K.M., and Rutishauser, U. (2017). Fixations gate species-specific responses to free viewing of faces in the human and macaque amygdala. *Cell Rep.* 18, 878–891.
72. Barnett, L., and Seth, A.K. (2014). The MVGC multivariate Granger causality toolbox: a new approach to Granger-causal inference. *J. Neurosci. Methods* 223, 50–68.
73. Sameshima, K., and Baccalá, L.A. (2022). asympPDC Package (Release v3.0.1 for File Exchange purpose, asympPDC/asympPDC, GitHub), GitHub.
74. Baccalá, L.A., and Sameshima, K. (2001). Partial directed coherence: a new concept in neural structure determination. *Biol. Cybern.* 84, 463–474.

STAR★METHODS

KEY RESOURCES TABLE

REAGENT or RESOURCE	SOURCE	IDENTIFIER
Critical commercial assays		
Eye tracking camera	SR Research	EyeLink 1000
Headpost	Grey Matter Research	N/A
Recording chamber	Rogue Research and Crist	N/A
16-channel axial array electrodes, U and V probes	Plexon Inc.	N/A
Single-channel electrodes	FHC	N/A
Multi-electrode Microdrive system	NaN Instruments	N/A
Neural recording data acquisition system	Plexon OmniPlex system	N/A
Deposited data		
Raw behavior and electrophysiology data	This paper	Upon request
Experimental models: organisms/strains		
<i>Macaca mulatta</i> monkeys	N/A	N/A
Software and algorithms		
MATLAB	Mathworks	2017a–2019b
Psychtoolbox	Brainard ⁶²	http://psychtoolbox.org/
EyeLink toolbox	Cornelissen et al. ⁶³	http://psychtoolbox.org/docs/EyelinkToolbox
EyeMMV toolbox	Krassanakis et al. ⁶⁴	https://github.com/krasvas/EyeMMV
MountainSort algorithm	Chung et al. ⁶⁵	https://github.com/magland/mountainlab
Codes	This paper	https://github.com/changlabneuro/dissoc-vicarious-received-reward [https://doi.org/10.5281/zenodo.7938480]

RESOURCE AVAILABILITY

Lead contact

Further information and requests for resources and reagents should be directed to and will be fulfilled by the lead contact, Steve W.C. Chang (steve.chang@yale.edu).

Materials availability

This study did not generate new unique reagents.

Data and code availability

Behavioral and neural data presented in this paper will be available upon request from the [lead contact](#). Original codes can be found at <https://github.com/changlabneuro/dissoc-vicarious-received-reward>.

EXPERIMENTAL MODEL AND SUBJECT DETAILS

Animals and surgery

A total of four adult male rhesus macaques (*Macaca mulatta*) were involved in the study. Two adult male macaques (monkeys K and H; ages, both 6-yr old; weights, 7 and 8 kg) functioned only as actors. Additionally, two adult female macaques (ages, 6 and 10-yr old; weights, 9 and 10 kg) were involved only as partners in the social reward allocation task. All animals were unrelated and not cage-mates. Actors were housed in a colony room with other males, but the two females resided in an adjacent colony room with other females. Although males and females did not live in the same colony room, they had multiple social interactions through previous experimental studies from the lab. While it is important to examine social relationship factors in the primate brain, our current study focused on first determining neuronal bases of signaling vicarious and experienced reward outcomes in the prefrontal-amygdala pathways in consistent pairings from the four animals used. With this foundational knowledge, future work can begin to examine

the neuronal modulations by social relationship factors underlying vicarious and experienced rewards in these pathways. All four monkeys were housed in pairs with other animals under a 12-hr light/dark cycle and had unrestricted food access and controlled fluid access during experiments. All four monkeys first received a surgically implanted headpost (Grey Matter Research) for restraining their head for eye-tracking and electrophysiology. The second surgery implanted recording chambers (Rogue Research and Crist) in actor monkeys to provide access to ACCg and BLA. All procedures were approved by the Yale Institutional Animal Care and Use Committee and in compliance with the National Institutes of Health Guide for the Care and Use of Laboratory Animals.

Anatomical localization

The location of the recording chambers was guided by both 3-Tesla structural magnetic resonance imaging (MRI; Siemens) and informed by stereotaxical coordinates of ACC and the amygdala. To directly map chamber-based coordinates of ACCg and BLA, manganese (Mn)-enhanced MRI (MEMRI) scans were performed. For both ACCg and BLA, we focally infused 2 μ l of 19.8 μ g/ μ l of MnCl₂ in saline solution using custom-modified Hamilton syringes lowered to the same trajectory as the recording electrodes. Following 3 hours of the Mn infusion, we performed a structural MRI scan and visualized a bright halo caused by the infused Mn.⁶⁶ All electrophysiological recordings were carried out simultaneously from both ACCg (Brodmann areas 24a, 24b, and 32)⁴⁶ and BLA⁴⁶ (Figure S1D). A different aspect of this dataset was used for a recently published study investigating the neuronal synchrony underlying prosocial and antisocial decision-making.³⁸

Social reward allocation task

An actor monkey and a partner monkey sat in primate chairs (Precision Engineering) with 100-cm distance between them at a 90° angle (Figure 1A). An empty bottle was placed exactly on the opposite side of the partner and was positioned at a comparable height to the face region of the partner monkey. A monitor, positioned directly in front of each monkey, displayed identical visual stimuli. Each monkey received juice drops from its own juice tubes controlled by two separate solenoid valves. Moreover, one additional juice tube controlled by its own dedicated solenoid valve delivered juice drops into the empty bottle. As in previous studies,^{27,29,35,38,44,45} all of these solenoid valves were placed in another room to prevent monkeys from forming secondary associations of solenoid clicks. White noise was also played during experimental sessions in the experimental room. An infrared eye-tracking camera (EyeLink 1000, SR Research) continuously recorded the horizontal and vertical eye positions at 1 kHz from actors who performed the task using gaze.

On each trial (Figure 1C), an actor began the trial by fixating on a central square for 150 ms using gaze. A vertical bar (magnitude cue) whose height indicated the juice volume at stake for that trial appeared in the center, mapped onto small (0.2 ml), medium (0.4 ml), and high (0.6 ml) juice sizes. The actor was continuously required to maintain fixation on the magnitude cue for 400 ms. Following a variable delay (200, 400, or 600 ms), the trial pseudo-randomly progressed into either a free-choice (75%) or a forced-choice (25%) trial. On a free-choice trial, two peripheral visual targets appeared at two random locations on opposite sides, at which time the actor was required to make a selection by shifting gaze to one of the targets within 2sec and maintaining the fixation for additional 150 ms to register the choice. On a forced-choice trial, one visual target appeared in the center, at which time the actor was required to fixate on it for 150 ms. Any break in fixation resulted in an incomplete trial with no further progress into the trial. The free-choice targets were always offered in two independent contexts (*Self/Both* and *Other/Bottle*), which were pseudo-randomly presented at equal frequency. Different visual target stimuli (mapped onto different reward outcomes) were used for different actors and different partners (an example set in Figure 1B).

In the *Self/Both* context (50% of free-choice trials), the actor chose between delivering a juice reward to himself (*Self*) or both himself and the partner at the same time for the same amount (*Both*) (i.e., the actor was always rewarded). In the *Other/Bottle* context (50% of free-choice trials), the actor chose between delivering a juice reward to the partner (*Other*) or to the juice collection bottle (*Bottle*) (i.e., the actor was never rewarded) (Figure 1B). Therefore, any choice in each context was 'reward-matched' for the actor. Following the choice, another variable delay ensued (200, 400, 600, or 800 ms) before a juice reward corresponding to the choice and the earlier magnitude cue was delivered. By contrast, on a forced-choice trial, the actor only saw a single target at the center of the screen mapped onto the reward to be delivered to the actor, *Self (Forced)*, the partner, *Other (Forced)*, both, *Both (Forced)*, or the bottle, *Bottle (Forced)* (Figure 1B). One of the four central targets was pseudo-randomly presented with equal frequency. Again, the actor had to remain fixated at this central target for 150 ms to complete the forced choice by the computer, with any break in fixation leading to an incomplete trial and no further progression into the trial. Identically to a free-choice trial, a variable delay (200, 400, 600, or 800 ms) ensued before a juice reward corresponding to the central target and the earlier magnitude cue was delivered to himself (*Self (Forced)*), the partner (*Other (Forced)*), both (*Both (Forced)*), and the bottle (*Bottle (Forced)*). For all trials, juice delivery was followed by a 2.5-sec inter-trial interval (free-viewing period), during which the actor looked around freely without any more task requirements. Only the data from completed trials were included in the analysis.

Electrophysiological recordings

Spiking activity and LFP recordings were performed using 16-channel axial array electrodes (U- or V-Probes, Plexon) or single tungsten electrodes (FHC Instruments) placed in each of the recording regions (i.e., two 16-channel arrays in both regions, or a 16-channel axial array in one region with a single channel in the other region) using the OmniPlex data acquisition system (Plexon). We also placed an additional independent subdural reference electrode as done previously.³⁸ In each recording session, a guide tube penetrated the

intact dura and guided the electrodes. Electrodes were lowered using a motorized multi-electrode tower microdrive (NaN Instruments) at a speed of 0.02mm/sec. Once the recording targets were reached, we waited 30min and began the data collection.

Method details

Behavioral choice analysis

To quantify social decision preferences, we constructed a choice preference index as contrast ratios^{27,35,38,44,45} (Equation 1).

$$\text{Preference Index} = \frac{R_a - R_b}{R_a + R_b} \quad (\text{Equation 1})$$

R_a and R_b were the frequency of chosen options. R_a and R_b were numbers of *Both* and *Self* choices or *Other* and *Bottle* choices in the *Self/Both* context or the *Other/Bottle* context, respectively. Thus, an index of 1 corresponds to always choosing a prosocial (positive other-regarding) outcome, -1 corresponds to always choosing an antisocial (negative other-regarding) outcome, and 0 indicates indifference. Choice reaction time, the time from the onset of two targets on free-choice trials to eye movement onset, was computed using a 20° sec⁻¹ velocity criterion. The frequency of looking at either the partner or the bottle was computed using the average number of gaze shifts landing on the partner's face, which was empirically mapped and fitted with a rectangle window, or the bottle, which was mapped empirically with the same-dimensioned window as the face region, during the 2.5-sec inter-trial interval. To compare the divergence times between *Other* and *Bottle* versus *Self* and *Both* for the continuous social gaze probability over time (2-ms resolution), we obtained times where the two mean traces differed by 4 SEM on each session and compared these distributions.

Spiking and local field potential (LFP) activity

We collected broadband analog signals which were amplified, band-pass filtered (250 Hz–8 kHz), and digitized (40 kHz) using the Plexon OmniPlex system. All collected spike data underwent waveform verifications offline and automatically sorted using the MountainSort.⁶⁵ LFP data were analyzed using the Chronux signal processing toolbox⁶⁷ and custom MATLAB scripts (The MathWorks). Continuous LFP voltages from each electrode in each area were segmented into 1-sec periods centered on the onset of reward delivery at a sample rate of 1 kHz. Raw voltage signals were then band-passed filtered from 2.5 Hz to 250 Hz. We chose a zero-phase filter to avoid introducing phase-distortions to the signals. Signals were normalized by subtracting a reference voltage trace recorded from an independent subdural reference electrode in order to eliminate common noise from each electrode, as done previously³⁸ (also see Bastos and Schoffelen⁶⁸). Crucially, it is also important to ensure that observed coherence was not confounded by the mouth movements of the actors on different reward outcome conditions. Because we were able to observe and verify localized mouth movement artifacts in LFP traces of the delta (1–4 Hz) and theta (4–8 Hz) frequency ranges (Figure S1E), we took a conservative approach and focused our data analyses on the frequency range above 10 Hz. Moreover, observed specificities in coherence patterns for free-choice trials compared to forced-choice trials support that potentially confounding factors associated with different reward outcomes per se were not likely to explain the results. For epoch-based analyses, we operationally defined the reward epoch to be 50–350 ms from reward onset for both free-choice and forced-choice trials.

Spike-field coherence between ACCg and BLA pairs

To quantify spike-field coherence, we designated one node in the ACCg-BLA pair as the spike contributor and the other node as the field contributor, and examined the phase differences between spike and LFP signals.^{38,48,68} As such, spike-field coherence was computed from two pairings, ACCg_{spike}-BLA_{field} coherence (pairing ACCg cells and BLA LFP sites) and BLA_{spike}-ACCg_{field} coherence (pairing BLA cells and ACCg LFP sites). Spikes and LFP signals were binned using sliding windows of 150 ms in steps of 50 ms for a 1-sec interval centered on reward onset for all trial types. We then computed Fourier estimates by a multi-taper transformation applied to single trial data, in which we selected a time half-bandwidth product of 2, and multiplied the raw signals by 3 Slepian (orthogonal) tapers,⁶⁹ yielding a frequency resolution of ~3.096 Hz with a 1 kHz sampling rate. We then additionally restricted the density estimates to the 10–60 Hz interval. The spectrum density of point process (spikes) was transformed by applying fast Fourier transform on the discrete data. Coherence was calculated between two spectrum densities of continuous process (LFP) and point process (spikes) by computing the cross-spectral density of the two processes (x and y ; P_{xy}) with respect to frequency (f), which was normalized by the product of the power spectral densities of each process (P_{xx} and P_{yy}) as a function of frequency (Equation 2).

$$\text{Coherence} = \frac{|P_{xy}(f)|^2}{P_{xx}(f)P_{yy}(f)} \quad (\text{Equation 2})$$

Raw coherence values therefore ranged from 0 to 1, where a perfectly constant phase relationship between ACCg cells or sites and BLA sites or cells, respectively, would be indicated by a coherence value of 1 while an absence of any phase relationship would be indicated by a value of 0. We contrasted coherence values between different conditions and obtained averages across pairs of cells and LFP sites. For actor_{norm} reward, coherence for *Self* and *Bottle* was first normalized by the mean of *Self* and *Bottle* (i.e., normalized by *Self* and *Bottle*), and then the contrast was generated. For partner_{norm} reward, coherence for *Other* and *Bottle* was first normalized by the mean of *Other* and *Bottle* (i.e., normalized by *Other* and *Bottle*), and then the contrast was generated. To examine the coherence levels separately for different reward magnitudes, we grouped trials into those with low, medium, and high juice sizes and repeated the same procedure.

For selecting coherence frequency ranges, we evaluated the specificity of time-frequency windows by considering the distribution of effects across frequencies and time. Specifically, we computed p-values of the test for *Self-Bottle* > *Other-Bottle* or *Other-Bottle* > *Self-Bottle* using time-frequency windows the same size as for the reported frequency ranges. For the alpha-beta frequency ranges, we did not observe any significant windows containing frequencies below 30 Hz except those adjacent to our reported time-frequency window (10–20 Hz, 50–250 ms from reward onset) or those substantially later (> 500ms post reward) or earlier (pre reward before time zero). For the gamma frequency ranges, other than the one we have chosen (35–51 Hz, 50–350 ms from reward onset), the only other differences were observed in higher frequencies but only long after the reward (> 450 ms). As our goal was to examine reward outcome processing, we considered these earlier and much later time periods more difficult to interpret because they reflect potentially confounding processes such as reward anticipation and post-reward outcome processes leading up to the next trial.

To obtain single-unit activity (SUA) ‘task space’ selectivity, we first computed trial-by-trial peri-stimulus time histograms aligned to the onset of reward on each trial, separately for each cell, in sliding windows of 150 ms stepped by 50 ms. We averaged firing rates over the reward epoch (50–350 ms relative to reward onset) and then calculated a series of coding metrics from subsets of the distribution of mean firing rates over trials, separately for each cell. The coding metrics comprised explained variance from two separate one-way ANOVAs as well as a depth of selectivity measure, such that each cell could be represented as a 3-dimensional vector. The first ANOVA considered activity on all trials as a factor of trial type (free-choice versus forced-choice trials), and the second ANOVA considered all trials as a factor of reward magnitude (low versus medium versus high). Thirdly, a measure of the depth of selectivity (DOS; Equation 3) was applied for outcomes (*Self*, *Other*, *Both*, *Bottle*), where n is the number of outcomes and Fr is the mean firing rate of each outcome.^{70,71} This produced, for total cells, a [cell count x 3] dimensional matrix on which we then performed PCA. We finally classified cell clusters from the PCA space matrix using k-means clustering with $k = 2$.

$$DOS = \frac{n - \frac{\sum(Fr)}{\max(Fr)}}{n - 1} \quad (\text{Equation 3})$$

Directionality of information flow (Granger causality and partial directed coherence)

To estimate the directionality of information between ACCg and BLA, we used two independent analyses to obtain converging results. First, we computed Granger causality using continuous LFP signals for *Self*, *Other*, and *Bottle* using the MVGC toolbox.⁷² Second, we computed spectral partial directed coherence (PDC) between the same LFP signals using the asympPDC toolbox.^{73,74} LFP signals were preprocessed in the same way for both analyses. Specifically, we first normalized raw ACCg and BLA signals sampled at 1 kHz by subtracting a reference voltage trace recorded simultaneously from an electrode placed in the dura, then filtered the raw signals with a zero-phase bandpass filter at 2.5 and 250 Hz.

We computed Granger causality, a spectral measure with values from 1–500 Hz stepped by 1 Hz, between pairs of simultaneously recorded ACCg and BLA sites. We computed Granger causality in sliding windows of 150 ms stepped by 50 ms aligned to reward onset, and separately for each set of trial conditions (i.e., separately for trial types and choice outcomes). We used a fixed model order of 32 and the default ‘LWR’ information criteria regression mode and computed site-by-site Granger values for *Self*, *Other*, and *Bottle* in the 10–20 Hz and 35–51 Hz frequency ranges. We computed PDC between the same sites and condition-subsets as for Granger causality, and again in sliding windows of 150 ms stepped by 50 ms aligned to reward-onset. The model order of the MVAR model was fixed at 30; this value was estimated to minimize AIC using a subset of $N = 16$ site-pairs. We computed spectral PDC in 128 frequency bins from 0–500 Hz — i.e., up to the Nyquist limit — then averaged separately over 10–20 Hz and 35–51 Hz frequency ranges.

Neuron, Volume 111

Supplemental information

**Dissociation of vicarious and experienced
rewards by coupling frequency
within the same neural pathway**

Philip T. Putnam, Cheng-Chi J. Chu, Nicholas A. Fagan, Olga Dal Monte, and Steve W.C. Chang

Supplemental Information

Supplemental Figure 1

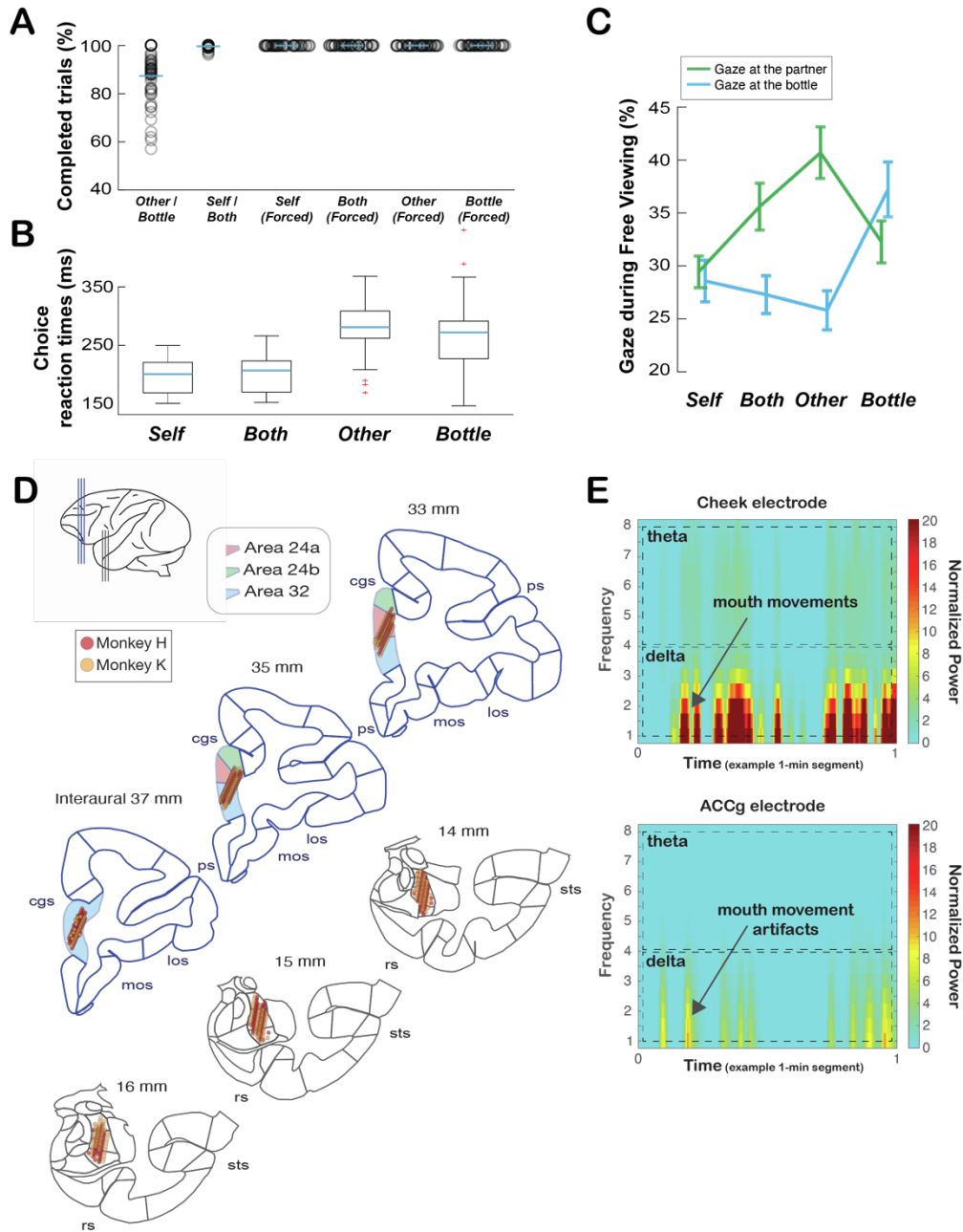


Figure S1. Additional behaviors, electrophysiological recording locations, and detection of LFP artifacts associated with mouth movements in the delta and theta frequency bands, related to Figure 1 and the STAR Methods. **A.** Average proportions of completed free-choice trials in the *Other/Bottle* and *Self/Both* contexts and completed forced-choice trials. Data points show individual sessions. Actors completed 99% of *Self/Both* trials and 87% of *Other/Bottle* trials. **B.** Choice saccade reaction times (mean \pm s.e.m.) for choosing *Self*, *Both*, *Other*, or *Bottle*. Reaction times differed as a function of choice ($F(3, 215) = 59$, $p < 0.0001$, on-way ANOVA), driven by the

differences in reaction times for receiving rewards (*Self* or *Both*) compared to forgoing rewards (*Other* or *Bottle*) ($p < 0.0001$, Wilcoxon rank sum; *Self* versus *Both*, *Other* versus *Bottle*, both $p > 0.75$; *Self* or *Both* versus *Other* or *Bottle*, all $p < 0.001$, Tukey test). **C.** Social gaze patterns reflected decisions to deliver juice rewards to the partner or the bottle as a function of different choices. Shown are the mean (\pm s.e.m.) proportions of gaze to the partner or to the bottle during the free viewing period for each reward outcome. Gaze patterns differed as a function of choice ($F(3, 455) = 2.86$, $p = 0.04$, two-way ANOVA) and gaze goal (the partner or the bottle; $F(1, 455) = 10.66$, $p < 0.005$, two-way ANOVA), with a strong interaction between choice and gaze goal ($F(3, 455) = 8.75$, $p < 0.0001$, two-way ANOVA). **D.** Recording locations of ACCg and BLA from monkey H (red points) and monkey K (orange points) projected onto the standard stereotaxic coordinates of the rhesus macaque brain atlas (with the Brodmann assignments of ACC according to the Paxinos atlas)⁴⁶. Shown are six representative coronal slices were (2-mm interaural spacing for ACCg and 1-mm interaural spacing for BLA) in the anterior-to-posterior dimension (top left cartoon). Selected landmarks: cingulate sulcus (cgs), principle sulcus (ps), medial orbitofrontal sulcus (mos), lateral orbitofrontal sulcus (los), superior temporal sulcus (sts), and rhinal sulcus (rs). **E.** (Top) Frequency over time plots from one independent session where signals were recorded from an additional electrode positioned on the cheek of a monkey for detecting mouth movements. Spontaneous mouth movements resulted in large increases in the lower frequency power in the delta and theta frequency ranges. (Bottom) Frequency over time plots obtained from the same example session from an ACCg electrode. Most of the mouth movements introduced LFP artifacts in the delta and theta frequency ranges.

Supplemental Figure 2

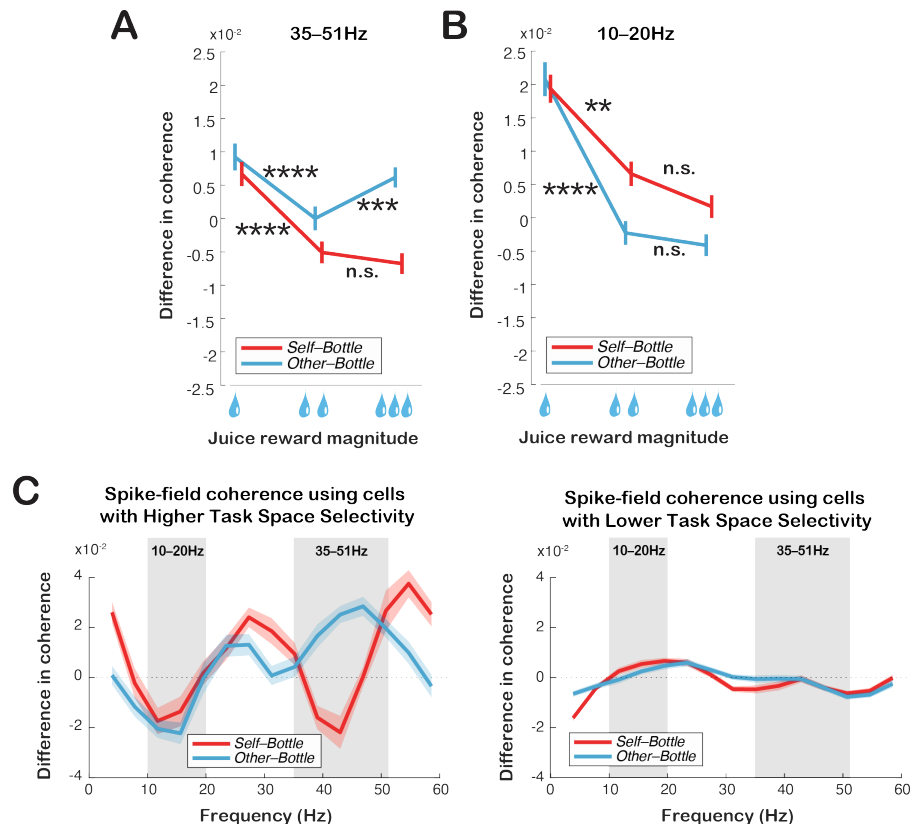


Figure S2. Effects of juice size on the $ACC_{g_{spike}}-BLA_{field}$ coherence in the gamma and alpha/beta frequency ranges, and difference in $ACC_{g_{spike}}-BLA_{field}$ coherence across frequency for the higher and lower task space selectivity cells, related to Figures 2 and 3. **A.** The gamma $ACC_{g_{spike}}-BLA_{field}$ coherence for partner_{norm} and actor_{norm} rewards on free-choice trials was modulated by juice size at stake. Shown are the gamma coherence for actor_{norm} and partner_{norm} rewards (mean \pm s.e.m.) separately for three juice sizes. **B.** The alpha/beta $ACC_{g_{spike}}-BLA_{field}$ coherence was modulated by juice size on free-choice trials. Shown are the alpha/beta coherence for actor_{norm} and partner_{norm} rewards (mean \pm s.e.m.) separately for the three juice sizes. In **A–B**, asterisks indicate significant differences between adjacent data points (****, $p < 0.0001$, ***, $p < 0.001$, **, $p < 0.005$, n.s., not significant; Wilcoxon rank sum). **C.** Shown are the differences in coherence (*Self-Bottle* in red and *Other-Bottle* in blue; mean \pm s.e.m.) from the higher task space selectivity cells (left) and lower task space selectivity cells (right) over frequency. In general, there were more coherence modulations for the higher task space selectivity cells than the lower task space selectivity cells. Notably, however, for the spike-field coherence from the cells with higher task space selectivity, the same gamma frequency range that exhibited the coherence bias for partner_{norm} reward also had the most robust differences in coherence between the two reward types compared to other frequencies. The grey windows show the two frequency ranges for reference.

Supplemental Figure 3

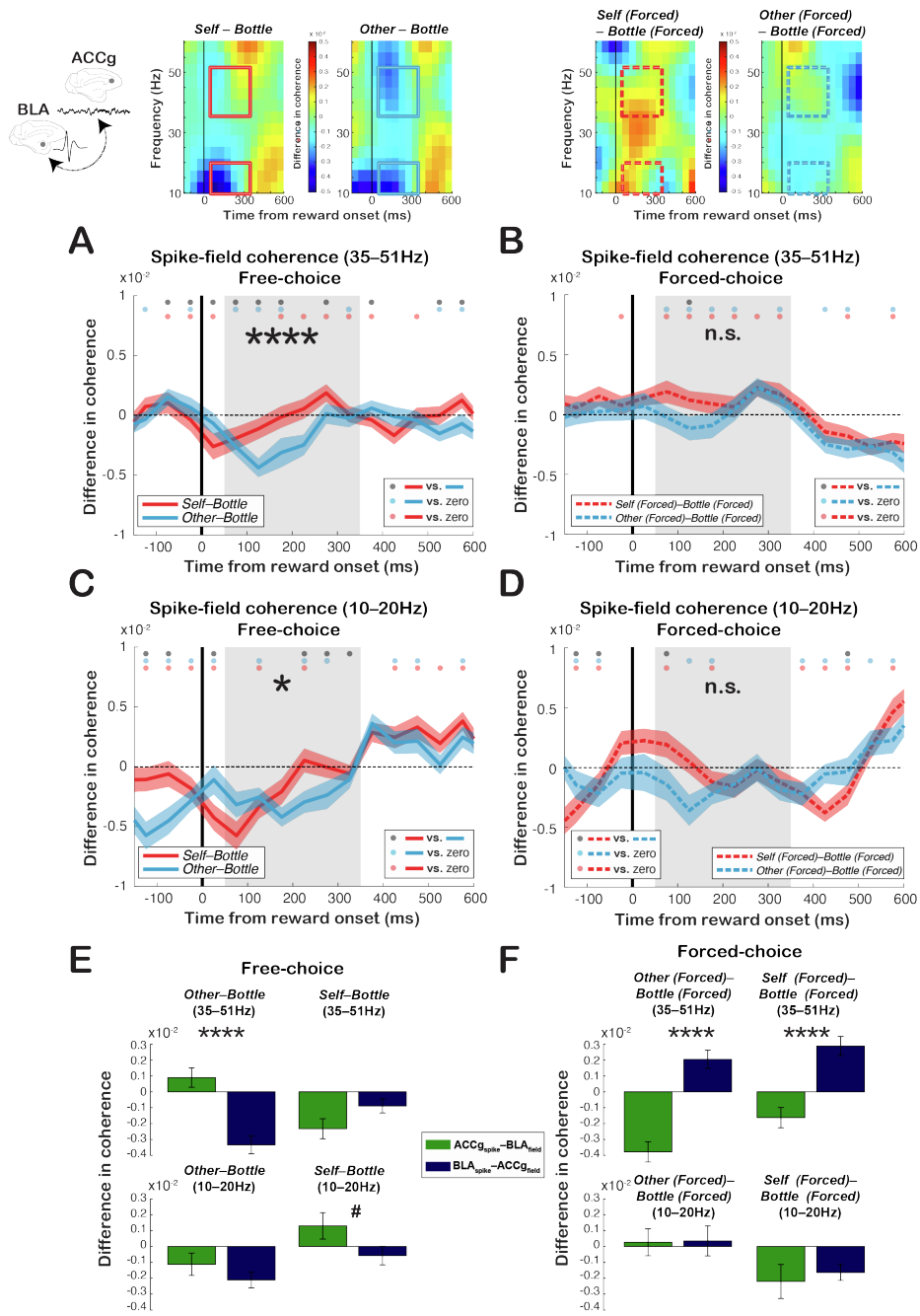


Figure S3. Spike-field coherence between spiking activity in BLA and LFP in ACCg (BLA_{spike}-ACC_{field}), related to Figures 2 and 3. A. Time courses of the gamma BLA_{spike}-ACC_{field} coherence (mean ± s.e.m.) for *Self-Bottle* (red) and *Other-Bottle* (blue) on free-choice trials (n = 842 pairs). **B.** Time courses of the gamma BLA_{spike}-ACC_{field} coherence (mean ± s.e.m.) for *Self (Forced)-Bottle (Forced)* (red) and *Other (Forced)-Bottle (Forced)* (blue) on forced-choice trials. **C.** Time courses of the alpha/beta BLA_{spike}-ACC_{field} coherence for *Self-Bottle* (red) and *Other-Bottle* (blue) on free-choice trials (n = 842 pairs). **D.** Time courses of the alpha/beta BLA_{spike}-ACC_{field} coherence for *Self (Forced)-Bottle (Forced)* (red) and *Other (Forced)-Bottle (Forced)* (blue) on forced-choice trials.

In **A–D**, circles at the top indicate unsmoothed raw time bins for the significant difference between the two traces (dark grey, $p < 0.05$, two-tailed t-test) as well as of each trace against zero (matching colors, $p < 0.05$). The shaded grey periods indicate the reward epoch. In all panels, asterisks indicate a significant difference between the two traces for the reward epoch (gray shading; 50–350 ms; ****, $p < 0.0001$, *, $p = 0.05$, n.s., not significant; two-tailed t-test). Top panels show the time-frequency spectrograms for all the conditions examined. Boxes (solid for free-choice trials and dashed for forced-choice trials) represent the frequency-time windows for the gamma and alpha/beta bands during the reward epoch. **E**. Direct magnitude comparisons between $ACC_{g_{spike}}-BLA_{field}$ and $BLA_{spike}-ACC_{g_{field}}$ coherence differences (mean \pm s.e.m.) for *Self–Bottle* and *Other–Bottle* on free-choice trials for the gamma and alpha/beta bands. **F**. Direct magnitude comparisons between $ACC_{g_{spike}}-BLA_{field}$ and $BLA_{spike}-ACC_{g_{field}}$ coherence differences (mean \pm s.e.m.) for *Self (Forced)–Bottle (Forced)* and *Other (Forced)–Bottle (Forced)* on forced-choice trials for the gamma and alpha/beta bands. In **E–F**, asterisks show significant differences between the two bars (****, $p < 0.0001$, #, $p = 0.06$, two-sample t-test).

Supplemental Figure 4

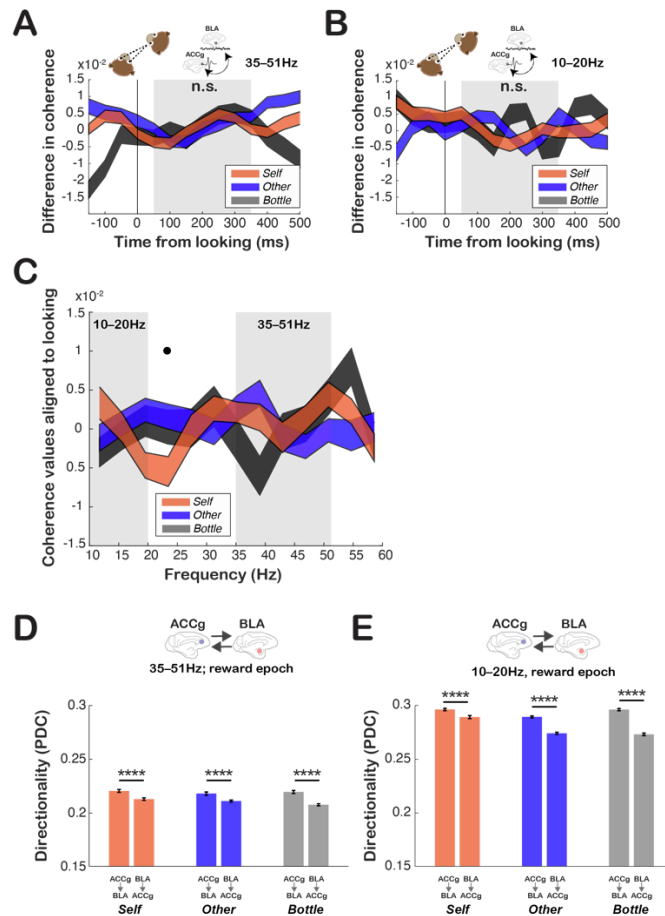


Figure S4. Social gaze effects on coherence for reward outcomes, and directionality biases for vicarious and experienced rewards in the ACCg-BLA pathway based on an alternative directionality measure, related to Figures 2, 3, and 4. **A–B.** ACCg_{spike}-BLA_{field} coherence for actor_{norm} and partner_{norm} rewards aligned to the onset time of looking events for the gamma (**A**) and the alpha/beta (**B**) bands on trials associated with *Self* (orange), *Other* (dark blue), and *Bottle* (dark grey) choices (mean \pm s.e.m.). The grey window indicates a comparable 50–350 ms window as the reward epoch (as used for aligning to reward onset). n.s., not significant, one-way ANOVA using *Self*, *Other*, and *Bottle*. **C.** ACCg_{spike}-BLA_{field} coherence values (mean \pm s.e.m.) for social gaze events (coherence aligned to the time of social gaze; 50–350 ms) across the frequencies examined. The black circle indicates a significant frequency bin with the main effect of reward outcome (non-overlapping bins frequency bins; $p < 0.05$, one-way ANOVA). The grey windows show the two frequency ranges for reference. **D–E.** Directionality results using the partial directed coherence (PDC). Average PDC values (mean \pm s.e.m.) of ACCg \rightarrow BLA and BLA \rightarrow ACCg directions from the reward epoch are shown for the gamma (**D**) and alpha/beta bands (**E**). Same format as **Fig. 4C–D** using the Granger directionality analysis. Asterisks indicate a significant difference between the two directions (****, $p < 0.0001$, n.s., not significant, two-tailed t-test).